analytical chemistry

pubs.acs.org/ac Article

Characterization of Glioblastoma Cancer Stem Cells Sorted by Sedimentation Field-Flow Fractionation Using an Ultrahigh-Frequency Range Dielectrophoresis Biosensor

Tarek Saydé, Rémi Manczak, Sofiane Saada, Gaelle Bégaud, Barbara Bessette, Gaëtane Lespes, Philippe Le Coustumer, Karen Gaudin, Claire Dalmay, Arnaud Pothier, Fabrice Lalloué, and Serge Battu*

Cite This: *Anal. Chem.* 2021, 93, 12664−12671 Read Online

ACCESS | Metrics & More | Article Recommendations | Supporting Information

ABSTRACT: Cancer stem cells (CSCs) appear to be an essential target for cancer therapies, in particular, in brain tumors such as Glioblastoma. Nevertheless, their isolation is made difficult by their low content in culture or tumors (<5% of the tumor mass) and is essentially based on the use of fluorescent or magnetic labeling techniques, increasing the risk of differentiation induction. The use of label-free separation methods such as sedimentation field-flow fractionation (SdFFF) is promising, but it becomes necessary to consider a coupling with a detection and characterization method for future identification and purification of CSCs from patient-derived tumors. In this study, we demonstrate for the first time the capability of using an ultrahigh-frequency range dielectrophoresis fluidic biosensor as a detector. This implies an important methodological adaptation of SdFFF cell sorting by the use of a new compatible carrier liquid DEP buffer (DEP-B). After SdFFF sorting, subpopulations derived from U87-MG and LN18 cell lines undergo biological characterization, demonstrating that using DEP-B as a carrier liquid, we sorted by SdFFF subpopulations with specific differentiation characteristics: F1 = differentiated cells/F2 = CSCs. These subpopulations presented high-frequency crossover (HFC) values similar to those measured for standard differentiated (around 110 MHz) and CSC (around 80 MHz) populations. This coupling appeared as a promising solution for the development of an online integration of these two complementary label-free separation/detection technologies.

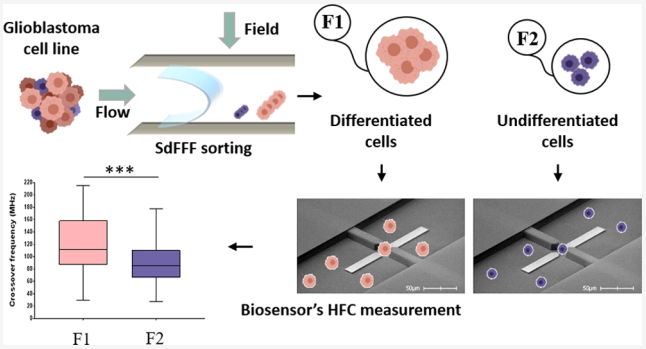

INTRODUCTION

Cancer stem cells (CSCs) are a key point and rare cell type found within a solid tumor, and they constitute 1−5% of the cells harboring the tumor niche.[1] CSCs are involved in three key processes that control tumor development.[2] First, it has been proven that CSCs can be involved in the growth and development of a tumor mass, because of their multipotency and self-renewal properties that mean the capacity to generate copies of themselves while simultaneously producing different types of differentiated cells.[3,4] Second, CSCs are also involved in metastatic dissemination. They are able to revert to an epithelial phenotype and thus promote tumor dissemination and metastasis to colonize distant organs.[5] Third, CSCs are known to be quiescent, a feature that helps them avert death caused by chemotherapy and radiotherapy.[6] This explains the fact that after initial reduction of the size of the tumor mass, cancer could be regenerated giving rise to relapses.[7,8] CSCs are present in numerous solid tumors such as Glioblastoma (GBM)[9] and are responsible for tumoral heterogeneity because of their stemness properties.[7] Because CSCs play a key role in tumor initiation, invasion, metastasis, and most importantly therapeutic resistance and therapy failure,[1−6] the design and development of new CSC-targeted therapies are of prime importance.[7,10] Thus, the CSC isolation is crucial for evaluating new therapeutic strategies. However, their characterization and isolation are still limited because of the small percentage of CSCs in the tumor niche or in the cell lines as well as their high plasticity.[10,11]

Classical approaches to characterize CSCs are phenotypic based on membrane marker expression such as CD133[12] and CD44[13] and intracellular or intranuclear marker expression such as Sox2,[14] Nanog,[15] and Oct4[16] They can also be functional like colony forming assays and orthotopic xenograft

Received: June 11, 2021
Accepted: August 24, 2021
Published: September 7, 2021

https://doi.org/10.1021/acs.analchem.1c02466
Anal. Chem. 2021, 93, 12664−12671

models on immunosuppressed mice.[17] Because of their plasticity, CSCs are often identified using more than one marker.[18] However, phenotypic changes take place often because of this reversible aspect because of their stemness features, promoting therefore a continuous change in the expression of CSC markers.[19] For example, CD133 was focused on as a major GBM CSC marker to the point where if a cell is CD133+, it is automatically considered as a CSC.[20] Other studies have proven that GBM CSCs are found to be CD133- but positive for other markers like Oct4 and Nanog, hence the need for a pool of markers to track down CSCs in a certain cell line.[21] Cell-sorting technologies such as fluorescence activated cell sorting and magnetic-activated cell sorting are mainly based on these markers to purify specific CSC subpopulations. However, the need for cellular labeling can induce functional changes consequently altering their stemness.[1]

In that way, label-free methods that ensure limited cellular changes in CSCs could be used. One of the most interesting label-free cell-sorting methods is the now well-known sedimentation field-flow fractionation (SdFFF) technique.[22−24] SdFFF is a gentle and noninvasive technique.[22] The advantage that SdFFF holds over other sorting techniques is the lack of need for immunolabeling.[22,25,26] It relies on cell biophysical properties: size, density, and rigidity. The cells are subjected in an empty ribbon-like separation channel (no stationary phase) to two types of forces (1) hydrodynamic lift forces generated by flowing a carrier liquid through the channel and (2) an external field applied perpendicularly to the flow direction.[22,23,27] Cells are then eluted under the "Hyperlayer" elution mode, a size/density driven separation mechanism, that ensures a drastic limitation of cell-solid panel interactions.

The end-goal of our work is to investigate the implementation of a label-free method to isolate and characterize CSCs simultaneously, serving as a diagnostic and prognostic approach, based on SdFFF cell sorting. Nevertheless, to perform both cell sorting and population characterization, there is not yet a hyphenated detector like what exists for the asymmetric field-flow fractionation (AF4) and multiangle light scattering for entities at a nanoscale.[28−30] Hence, after SdFFF cell sorting, the subpopulations of cells undergo offline biological characterization. Even though they are effective for routine preparation of CSCs from the cell line and primary cell culture,[23] they are cost- and time-consuming and not adapted for CSCs isolated from a highly variable and heterogeneous population, for example, patient-derived tumor samples. To overcome this limitation, a hyphenation of the SdFFF with a label-free based biosensor as a postsorting online characterizing detector was investigated.

A first step of the development of this solution was previously published,[23] which consisted of a combination approach of the SdFFF with a microwave dielectric spectroscopy technique. The latter is based on resonance disturbance principles, corresponding to the microwave range of the electromagnetic spectrum, and permits characterization of cell contents and a mean to discriminate and analyze cells. This technique discriminates between different subpopulations having opposite differentiation status by relying on their intrinsic intracellular dielectric permittivity.[23] While SdFFF combined with a dielectric spectroscope proved its potential to sort and characterize subpopulations of GBM cell lines, this approach's major limitation resides in the need for fixating cells before introducing them individually between electrodes in a dry nonfluidic system.[23] Therefore, the investigated dead cells can no longer be used in further analysis.

This the reason why we aim to improve the post-SdFFF characterization on living cells, by combining SdFFF with a new ultrahigh-frequency range dielectrophoresis (UHF-DEP) biosensor.[31] UHF-DEP is a label-free, accurate, fast, and low-cost characterization method that uses the principles of polarization (in the ultrahigh-frequency range from 50 up to 600 MHz) and the motion of living cells in applied electric fields: DEP cell electromanipulation inside a microfluidic device.[31] UHF-DEP characterization brings information about the individual cell cytoplasm content own physical property (dielectric), without lyse or implied denaturation. The DEP buffer (DEP-B) used as a carrier liquid for the UHF-DEP is an osmotic sucrose-based survival buffer. Previously, two subpopulations of GBM cell lines, one enriched with CSCs by cultivating the cells in a gold standard define medium (DM) and another cultivated in a normal medium (NM) with a high percentage of differentiated cells, were discriminated using UHF-DEP.[31] The population with a high percentage of CSCs (in DM) exhibited lower high-frequency crossover (HFC) values than that of a population with a high percentage of differentiated cells (in NM). In this manner, we now consider the HFC or electromagnetic signature as a marker for CSC discrimination, confirming the UHF-DEP biosensor's potential.[31]

The foreseen target of this work is an online hyphenation of SdFFF and the biosensor. In this paper, we have to prove, via an offline coupling, the compliance between cell sorting by SdFFF and the characterization by UHF-DEP. In view of a future online hyphenation, it was logical to use from this point forward one common carrier liquid for both systems. The choice is made on the buffer compatible with the detector, DEP-B, which implies the validation of the elution conditions by SdFFF with DEP-B as a carrier liquid instead of the usually used phosphate buffer solution (PBS).[23] After cell sorting by SdFFF with this new carrier liquid, cell subpopulations undergo biological characterization, generating populations enriched or not in CSCs. The HFC values of each subpopulation were measured by UHF-DEP by comparison to a gold standard. The HFC values of the SdFFF subpopulation enriched in CSCs are similar to those of the reference population, proving the validity of this approach and the practical application of the future online hyphenation and its clinical relevance in the future.

MATERIALS AND METHODS

Schematic representations of the offline hyphenation of SdFFF and UHF-DEP biosensor are presented in Figure SI-1.

Cell Culture. The human GBM cell lines U87-MG and LN18 were purchased from the American Type Culture Collection (ATCC, Manassas, VA, USA) and grown under two conditions: NM (normal medium with fetal bovine serum) and DM (define medium [serum-free]). The schematic representation of the experimental conditions is represented in Figure SI-2. The NM and DM compositions are previously described.[23] Cell culture is conducted at a 500×10^3 density rate for 72 h for U87-MG and 750×10^3 for 48 h for LN18. After culture time, cells are dissociated using versene solution (Thermofisher scientific, France) and centrifuged at 300 g for 5′. Cells are then resuspended in DEP-B, an ion-free osmotic medium TRIS buffer-based, composed of a water/sucrose mixture with magnesium chloride (pH: 7.4; conductivity: 26

https://doi.org/10.1021/acs.analchem.1c02466
Anal. Chem. 2021, 93, 12664−12671

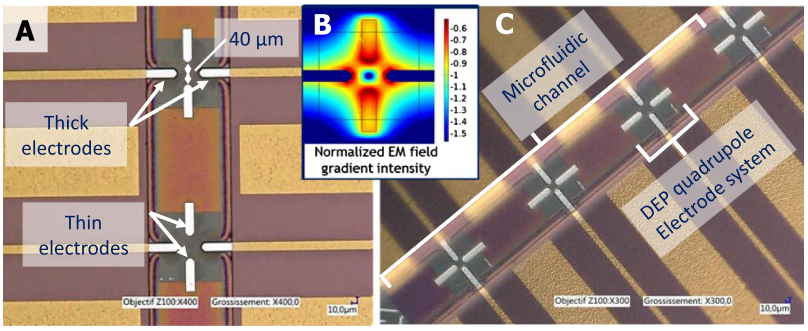

Figure 1. UHF-DEP detector: (A) Top view of the quadrupole electrode sensor used for HFC frequency measurement. Two types of electrodes are present, thin (top and bottom) and thick (left and right), with a gap of 40 μm. (B) Simulated electric field into the DEP quadrupole electrode system. (C) Angle view through the PDMS cap of the sensor array under the PDMS cap implemented at the bottom of a microfluidic channel.

mS/m) conventionally used for DEP experiments.[31] Cells are then counted using trypan blue (Sigma) exclusion and a Malassez cell counting chamber. The volume is adjusted to obtain 2.5 × 10^6 cells per 1000 μL.

SdFFF Device and Cell Elution Conditions. The SdFFF separation device used in this study was previously described.[23] Optimal elution conditions were as follows: flow injection through the accumulation wall of a 100 μL U87-MG and LN18 cell suspension (2 × 10^6 cells/mL). Flow rate: 1.0 mL/min. Carrier liquid: sterile DEP-B, pH 7.4 and conductivity 24 mS/m. External multigravitational field strength: 15 g for U87-MG (312.5 rpm) and 25 g for LN18 (402.5 rpm) ± 0.2 g. Time-dependent fraction collection: **F1**: 2′40″ to 4′20″ for U87-MG; and 2′30″ to 4′45″ for LN18. **F2**: 5′55″ to 8′00″ for U87-MG; and 8′30″ to 12′00″ for LN18. **TP** (total peak: fractions constituting the collection of the total eluted population (except the void volume, see Figure 2) as an internal control): 2′00″ to 8′00″ for U87-MG; from 2′00″ to 12′00″ for LN18. The crude population constitutes the remaining unsorted cell suspension that is used as the external control population. To obtain a sufficient quantity of cells for further analysis and subculture, consecutive (10−12 injections) SdFFF fraction collections were performed.

Tools and Methodology for Cell Crossover Frequency Measurement. In this study, we aim to characterize subpopulations of GBM cell lines subsequent to their sorting, by measuring their crossover frequencies in the ultrahigh-frequency range. The measurement process was fully described previously.[31] It consists of subjecting individual cells to a high-frequency electric field and monitoring under a microscope, while tuning by signal frequency, the induced cell motion. When cells are subjected to negative DEP forces, they are repelled; in contrast, they are attracted by a positive DEP force. When the electric field frequency reaches the cell crossover frequency, the DEP force becomes null, and it can be measured from the optically observable cell change of motion behavior.

For the present study, a dedicated microfluidic chip has been used based on aluminum passivated microelectrodes forming a 90° quadrupole sensor (Figure 1A). This sensor has been implemented on a *@IHP Innovations for High Performance Microelectronics* BiCMOS silicon technology substrate, diced into a cm^2 chip, and packaged with a polydimethylsiloxane (PDMS) cover to form a 200 μm wide and 40 μm high microfluidic channel above the sensor (Figure 1C). As shown in Figure 1, led experiments were performed using a 40 × 40 μm gap electrode design that combines a pair of thick electrodes (9 μm, see Figure 1A and Figure SI-1B) that crossed the microfluidic channel width, with another pair of thin electrodes (0.45 μm, Figure 1A) implemented in the middle of the channel where most of the cells flow (Figure 1C). Such design allows the generation of an electric field gradient configuration presenting a very localized low-magnitude field spot in the middle of the structure on the contrary with high-magnitude barriers surrounded by electrode edges (Figure 1B simulated electric field insert). Hence properly biasing the left and right electrodes with a high-frequency signal, whereas top and bottom ones are grounded, it is hence possible to form an efficient electrical trap to catch biological cells flowing in the main central channel part (Figure SI-1B). The sensor is biased through 50 Ω (10 μm wide) microstrip lines implemented under the PDMS cap until the chip edges thanks to a microwave signal generator (R&SSMB100A) associated with a wide band amplificator (Bonn Elecktrik BLWA 110-5M). We were able to generate a high-purity continuous wave signal with magnitude up to 10 Vpp. For the current experiment, the typically used magnitude of the applied voltage ranges between 2 and 4 Vpp.

Cellular Characterization. A complete description of the phenotypical and functional characterization of cell subpopulations is shown in the Supporting Information (see SI-1 and SI-2).

Analysis of Cell Size Using a Coulter Counter. Cell size means of different populations are measured subsequent to SdFFF cell sorting.

RTqPCR. mRNA expression levels of CSC markers are evaluated in the different populations.

Soft Agar Clonogenic Assay. A method used to test the ability of the cells to form clones in soft agar. CSCs are known to have high clonogenic properties by comparison to differentiated cells.

DNA Cell Cycle Analysis. A method that most frequently employs flow cytometry to distinguish cells in different phases of the cell cycle: CSCs are known to be quiescent hence in the G1 phase whereas differentiated cells are proliferative and ready to undergo mitosis hence tend to be in the G2 phase.

Statistical Analysis. Statistical analysis were performed on three independent experiments using Prism graphpad. Analysis of variance (ANOVA), Student's *t*-test, and Mann−Whitney test were conducted to compare different conditions. *P* values of ≤0.05 were considered statistically significant.

RESULTS AND DISCUSSION

Methodological Development of SdFFF Cell Sorting. *SdFFF with DEP-B as a Carrier Liquid.* In the goal of

https://doi.org/10.1021/acs.analchem.1c02466
Anal. Chem. 2021, 93, 12664−12671

combining SdFFF and UHF-DEP, which are two fluidic devices having each their own carrier liquid, we decided to use the detector compatible carrier liquid, the DEP-B, because UHF-DEP is not operational with PBS because of the high content of salt whereas SdFFF could be investigated with either DEP-B or PBS as a carrier liquid.

Nevertheless, the use of DEP-B as the carrier liquid for SdFFF requires a new methodological development and validation step for SdFFF cell sorting. The presence of sucrose (8.5%[31]) in the DEP-B medium leads to an important change in the elution profile of U87-MG and LN18 (Figure 2), most

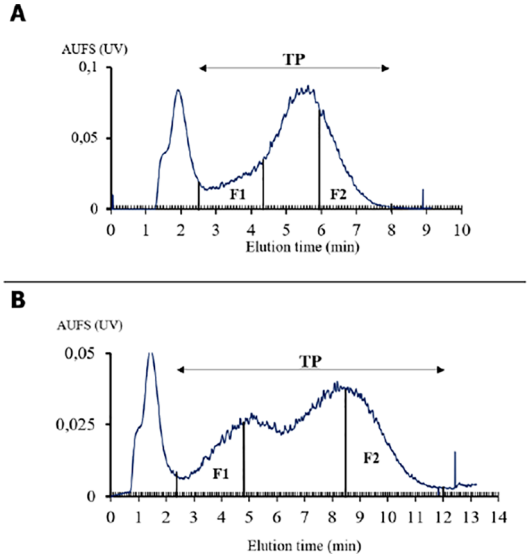

Figure 2. SdFFF fractograms of cells cultured in NM prior to sorting: (A) U87-MG cell line, carrier liquid: sterile DEP-B; (B) LN18 cell line, carrier liquid: sterile DEP-B. Elution conditions flow and field 1.0 mL/min and 15 or 25 g for U87-MG and LN18, respectively. Time-dependent fraction collections: see the Materials and Methods section.

likely because of the slight change in density (PBS: 1.0034/DEP: 1.031). A better resolution of cell peak vs dead volume peak, facilitating fraction collection, was observed (Figure 2A,B). This is particularly true concerning U87-MG compared to previously published fractograms.[23] These profiles also present reproducibility and repeatability with CV < 5% in terms of elution time. Finally, the cell viability throughout the conservation of cells in DEP-B remains higher than that observed in PBS for both cell lines (see Table SI-1).

The usually described SdFFF elution mode for cells is the "hyperlayer" mode[22,23,32,33] in which subpopulations of cells are focused into a thin layer at an equilibrium position in the channel thickness, depending on their biophysical properties: size and density as first-order parameters, along with shape and rigidity.[24] The hyperlayer elution order is size- and density-dependent: larger and less dense cells are focused in the faster streamlines and are consequently eluted first. The experimental retention ratio, R_{obs} (void time divided by retention time [t_0/t_R], measured by the first moment method),[34] was calculated to determine the average velocities and elution modes.

Under our elution conditions (see the Materials and Methods section), we obtained for both cell lines, fractograms with two (U87-MG) or three (LN-18) (Figure 2A,B) major peaks, the first corresponding to nonretained species (void volume peak, $R_{obs} \approx 1$), and the second (and third) corresponding specifically to cell subpopulations with $R_{obs} < 1$ (see below).

The hyperlayer elution mode was first determined based on the field and flow rate dependence of R_{obs}.[23,27,32,33] Then, at equivalent flow rates, the increase in field strength focused cells in slower stream lines, increasing retention and decreasing R_{obs}. In that way, U87-MG showed a decrease in R_{obs} of 33% by increasing the field from 10 to 20 g and 13% for LN18 by increasing the field from 20 to 30 g. This low difference could be explained by the fact that LN18 was eluted with higher field strength.

In the hyperlayer elution mode, samples were lifted away from the accumulation wall, limiting harmful cell−surface interactions. Using the following equation[35]

$$s = \frac{R_{obs} \times \omega}{6}$$

in which ω is the channel thickness (175 μm), we calculated the value of s, the average distance from the center of the cell to the channel wall,[35] which should be greater than the particle radius r, calculated from the mean cell diameter. The mean R_{obs} value calculated for U87-MG is 0.361 ± 0.004 and 0.273 ± 0.004 for LN18, leading respectively to s = 10.5 μm and s = 8.0 μm. These values appeared greater than the mean radius measured using a Coulter counter (see the Materials and Methods section) on the total peak population which are 8.0 μm for U87-MG and 7.0 μm for LN18.

Finally, the hyperlayer elution mode relies mainly on biophysical properties of the cell such as the cell size and density.[22,23,27,32] As described before, bigger and less dense cells are eluted in first, whereas smaller and denser cells are eluted last. Subsequent to their sorting and fraction collection (see the Materials and Methods section), the mean of the subpopulation size was investigated using a Coulter counter. The F1 fraction displayed a significantly higher size mean than that of the F2 fraction with a difference of Δd = 1.9 μm for U87-MG (Figure 3A) and Δ = 2.7 μm for LN18 (Figure SI-3A). Then according to the results of R_{obs} variation, s measurement, and size variation, we can assume that cells are eluted under hyperlayer elution using DEP-B as a carrier liquid.

Nevertheless, a major change in the elution parameters such as changing the carrier liquid requires a series of biological characterization methods for both cell lines to validate the SdFFF's efficiency to sort CSCs.

Phenotypical Characterization. CSC plasticity results in an intratumoral heterogeneity observed in solid tumors such as GBM.[36] For this matter, evaluating the expression of one marker is not enough to conclude on stemness properties, but a pool of CSC markers is mandatory. Many markers have been identified to be overexpressed in CSCs such as the transcription factors Sox2,[14] Nanog,[15] and Oct4.[16,23] This increase in expression is often evaluated at a transcriptomic levels. Differential analysis of CSCs mRNA expression levels was assessed in the subpopulations F1 and F2 by RTqPCR for U87-MG and LN18 cell lines. All three CSC markers (Oct4, Sox2, and Nanog) for U87-MG are significantly overexpressed in F2 enriched in undifferentiated cells compared to F1 enriched in differentiated cells: 3.5 fold higher in F2 than F1 for Oct4, 3.2 fold higher in F2 than F1 for Sox2, and 5.6 fold higher in F2 than F1 for Nanog (Figure 3B, see Figure SI-3B for LN18). The overexpression of CSC markers confirms that the F2 cell subpopulation is efficiently enriched in CSCs.

https://doi.org/10.1021/acs.analchem.1c02466
Anal. Chem. 2021, 93, 12664−12671

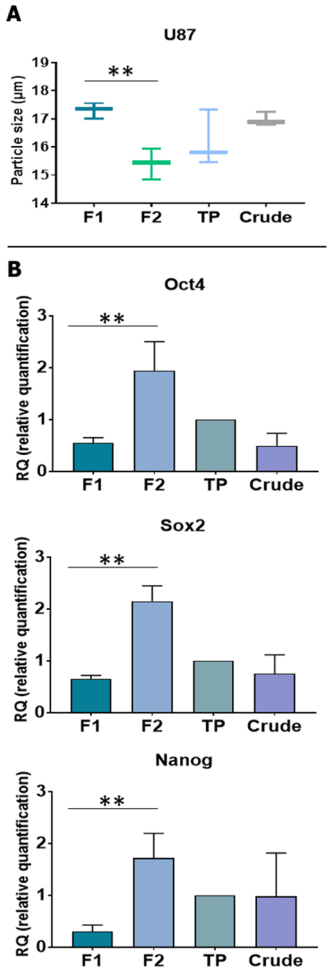

Figure 3. Phenotypical characterization of the different subpopulations of U87-MG sorted by SdFFF. (A) Biophysical property: cell size analysis by Coulter counter of post-SdFFF populations (F1, F2, TP, and crude) and (B) comparative analysis of gene expression of three CSC markers: Oct-4, Sox2, and Nanog, in the U87-MG cell line, of the post-SdFFF populations (F1, F2, TP, and crude), measured by real-time quantitative polymerase chain reaction (PCR) and normalized compared to TP. (see SI-1) The p value was determined using the t Student test or Mann−Whitney test. ** represents p value < 0.001.

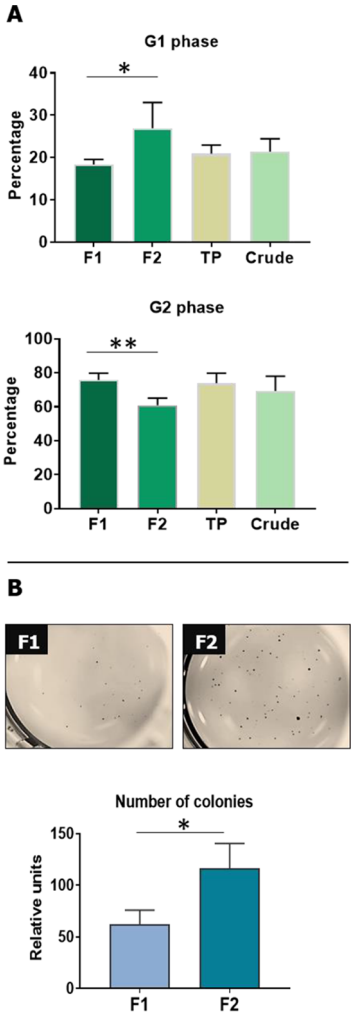

Figure 4. Functional characterization of the different subpopulations of U87-MG sorted by SdFFF (A) Cell cycle analysis by DNA content measurement: showing that CSCs (F2), the quiescent cells, are more likely found in the G1 phase, vice versa to differentiated cells. (B) Soft agar assay for colony formation examination evaluating the subpopulation capacity to form clones when cultured in soft agar (see SI-2). The p value was determined using the t Student test. ** represents p value < 0.001 and * represents p value < 0.05

CSCs tend to remain quiescent within the tumor niche so they can maintain their multipotency, consequently the main source supplying tumor growth.[37,38] For this matter, CSCs are often found at the G1 phase of the DNA cell cycle, also known as the quiescence phase, whereas differentiated cells, the more mature and ready to proliferate, are found at the G2 phase, also known as the growth phase.[39] Our DNA cell cycle analysis showed a higher tendency for the U87-MG F1 subpopulation to be in the G2 phase of the cell cycle, while the U87-MG F2 subpopulation enriched in CSCs is found to be in the G1 phase (Figure 4A, see Figure SI-3C for LN18). This confirms that we have managed to isolate and enrich a subpopulation of cells having high stemness characteristics as revealed in transcriptomic and cell cycle analysis.

Functional Characterization. CSCs have the capability to form an important quantity of colonies because of their self-renewal properties.[17] Soft agar colony formation assay is considered as one of the most rigorous and effective techniques for evaluating this capability in vitro[40] and characterizing stemness properties of cells.[41]

Our soft agar assay shows that the U87-MG F2 subpopulation managed to form a high number of colonies within 30 days of culture in soft agar, therefore exhibiting a stem-like behavior unlike U87-MG F1 (Figure 4B, see Figure SI-3D for LN18). This test validates the functional aspect of the CSC population.

This series of biological characterization proves that, after cell line culture in NM, the F2 subpopulation consists of a population of cells enriched in CSCs, whereas the F1 subpopulation is enriched in differentiated cells for both U87-MG and LN18 cell lines. Therefore, the SdFFF is validated as a cell-sorting label-free method using DEP-B as a carrier liquid instead of PBS.

Cell Characterization with the UHF-DEP Biosensor Subsequent to Their Sorting. *Crossover Frequencies of GBM Cells Cultured in NM before SdFFF.* The SdFFF technique has proven its potential to isolate a population

https://doi.org/10.1021/acs.analchem.1c02466
Anal. Chem. 2021, 93, 12664−12671

enriched in CSCs using the DEP-B as a carrier liquid. To validate the possibility of an association between SdFFF and UHF-DEP, the subpopulations (F1, F2), TP, and crude of the two GBM cell lines, U87-MG and LN18, were characterized by measuring their HFC values with UHF-DEP. The HFC considered corresponds to the frequency at which the trapped cell begins to move away from the center of the quadrupole electrodes (see Figure SI-2 for abbreviations and experimental conditions).

In previous work, it has been demonstrated that the more the population is enriched in CSCs, the lower the HFC values of the cells are, by comparison to differentiated cells cultured.[31] In the same way, we cultured in this study the two GBM cell lines (U87-MG/LN18) in NM and in the DM known to enrich the population in CSC.

First, the subpopulations of U87-MG and LN18 cultured in NM sorted by SdFFF with DEP-B were characterized by the UHF-DEP biosensor. As shown in Figure 5A and Table SI-2, for U87-MG, the median HFC value of the F1 subpopulation (U87-MG F1 NM) is similar to that of the unsorted cells cultured in NM (U87-MG NM) (respectively 103 and 111 MHz), whereas the median HFC value of the F2 subpopulation (U87-MG F2 NM) is similar to that of the unsorted cells cultured in DM (U87-MG DM) (respectively 81 and 85 MHz). Similar results were observed in Figure SI-4 and Table SI-2, with LN18 where the median HFC value of the F1 subpopulation (LN18 F1 NM) is similar to that of the unsorted cells cultured in NM (LN18 NM) (respectively 109 and 119 MHz), whereas the median HFC value of the F2 subpopulation (LN18 F2 NM) is similar to that of the unsorted cells cultured in DM (LN18 DM) (respectively 74 and 77 MHz).

This finding indicates that the subpopulations F1 and F2 sorted by SdFFF with DEP-B as a carrier liquid exhibited crossover frequencies respective of differentiated cells for F1 and CSCs for F2. These results obtained with an offline approach validate the relevance of an online hyphenation of SdFFF as a cell-sorting technique and UHF-DEP as a postsorting detector.

Thus far, all of these characterization studies have been performed on cells cultured in NM prior to their sorting by SdFFF with DEP-B. However, as previously done,[23] we wanted to examine the possibility of purifying even further the population of CSCs, by cultivating the cells in DM, sorting the population with SdFFF, and finally characterizing the generated subpopulations by UHF-DEP. Both cell lines were cultured in DM for 6 days and then sorted by SdFFF with DEP-B (see Figure SI-5).

The median HFC value of the F1 subpopulation post DM culture (U87-MG F1 DM) is 81.5 MHz and that of the F2 subpopulation post DM culture (U87-MG F2 DM) is 73 MHz. Both HFC values are very close to that of the previously measured U87-MG F2 NM population (81 MHz) (Figure 5B, see Table SI-2). This result was expected because even before cell sorting, the entire population was highly enriched in CSCs because of the DM; therefore, both subpopulations are equally enriched in CSCs. Similar results were obtained with LN18 where the median HFC value of LN18 F1 DM is 80 MHz and LN18 F2 DM is 72 MHz, similar to that of the unsorted cells cultured in DM (LN18- DM) with a median of 77 MHz (see Figure SI-4 and Table SI-2).

These results indicate that the SdFFF has successfully managed to purify to the highest extent a subpopulation

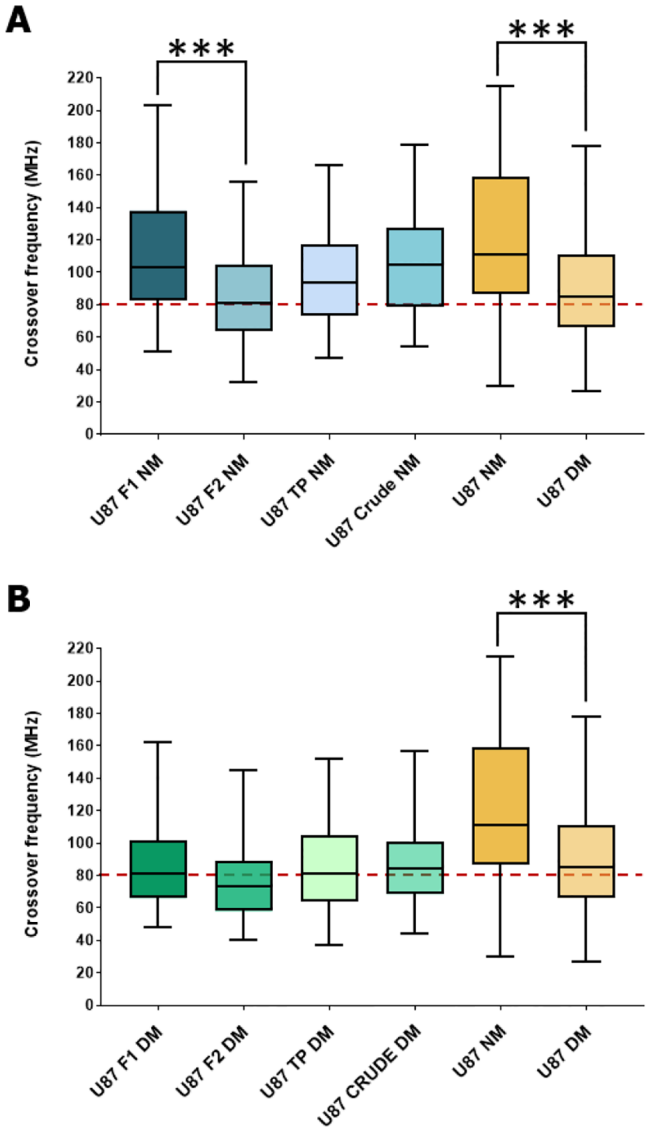

Figure 5. Graphic box plot representation of the HFC values of U87-MG cells (A) cultured in NM and sorted by SdFFF (U87 F1 NM and U87 F2 NM); (B) cultured in DM and sorted by SdFFF (U87 F1 DM and U87 F2 DM). Cells cultured in NM and DM without sorting (U87 NM and U87 DM). The red threshold represents the median of U87-MG F2 NM. The p value was determined using the one-way ANOVA test. *** represents p value < 0.0001.

enriched in CSCs. It conveys a population sorted by SdFFF and is characterized by the UHF-biosensor without the need for a DM for CSC enrichment. In addition, the NM conserves the heterogeneity of the CSC population. The clear advantage that was observed is that the cells cultured in NM maintain a high viability rate (95% for U87-MG and 93% for LN18) after SdFFF cell sorting with UHF-B, whereas cells cultured in DM before SdFFF are subjected to highly stressful conditions that result in a significative decrease in cell viability (60% for U87-MG and 40% for LN18). The preservation of this high viability of CSCs after normal elution conditions by SdFFF opens the door to a wide variety of applications, most importantly the design of diagnostic approaches, targeted therapies, and a deeper understanding of CSCs in general.

https://doi.org/10.1021/acs.analchem.1c02466
Anal. Chem. 2021, 93, 12664−12671

CONCLUSIONS

Unlike other types of FFF separation techniques, SdFFF used as a cell sorter lacks online label-free characterization. In previous studies, an association between SdFFF and a label-free detector has been investigated.[23] This approach failed to maintain cell viability after characterization. For this matter, in this study, we aimed to investigate a possible association between SdFFF and a microfluidic label-free biosensor in the ultrahigh-frequency range. Both SdFFF and the UHF-DEP biosensor have individually proven their potential to respectively sort and characterize cells without labeling while maintaining high cell viability. First, this coupling required a compatibility investigation between both techniques that revealed the need for a methodological development of SdFFF to adapt to the detector. By unifying the carrier liquid for a DEP-B compatible medium, our work has shown that the SdFFF was capable of sorting two subpopulations of GBM cell lines having opposite states of differentiation. All the physical and biological parameters studied (phenotypical and functional) proved the enrichment of CSCs in the F2. The HFC values of the subpopulations subsequent to FFF sorting showed a unique HFC to each population similar to that of gold standard measurements. This study aims to prove the feasibility and re-adaptation of the separation method to be compatible with the detection method. These two label-free techniques allowed cell separation on the basis of orthogonal properties: size, density, shape, rigidity for FFF, and the dielectrophoretic properties for UHF-DEP, for the diagnostic management of complex tumor populations originating from the patient. In the context of application using patient-derived cells, it is practically impossible to use a gold standard medium such as the DM to enrich the population in CSCs. Therefore, an online device SdFFF/UHF-DEP is inevitable for these sorts of applications and analysis. An ongoing development consists of determining the setting up of one single fast, low-cost, and effective tool that enhances the evaluation of CSCs in tumors opening the door to novel diagnostic, prognostic, and theranostic approaches.

ASSOCIATED CONTENT

Supporting Information

The Supporting Information is available free of charge at https://pubs.acs.org/doi/10.1021/acs.analchem.1c02466.

> Description of phenotypical and functional characterization of cell subpopulations, figures for schematic representations of both technique's offline coupling, for experimental conditions of cell culture, figures for phenotypical and functional characterization of LN18 cell line, fractograms in DM conditions, cell viability, and finally a table with the values of HFC (PDF)

AUTHOR INFORMATION

Corresponding Author

Serge Battu − *EA3842-CAPTuR, GEIST, Faculté de Médecine, Université de Limoges, Limoges 87025, France;* orcid.org/0000-0003-1861-9410; Email: serge.battu@unilim.fr

Authors

Tarek Saydé − *EA3842-CAPTuR, GEIST, Faculté de Médecine, Université de Limoges, Limoges 87025, France; ARNA, INSERM U1212, UMR CNRS 5320, Université de Bordeaux, Bordeaux 33076, France;* orcid.org/0000-0002-7377-394X

Rémi Manczak − *XLIM-UMR CNRS 7252, Université de Limoges, Limoges 87060 LIMOGES CEDEX, France*

Sofiane Saada − *EA3842-CAPTuR, GEIST, Faculté de Médecine, Université de Limoges, Limoges 87025, France*

Gaelle Bégaud − *EA3842-CAPTuR, GEIST, Faculté de Médecine, Université de Limoges, Limoges 87025, France*

Barbara Bessette − *EA3842-CAPTuR, GEIST, Faculté de Médecine, Université de Limoges, Limoges 87025, France*

Gaëtane Lespes − *CNRS, Institut des Sciences Analytiques et de Physico-Chimie pour l'Environnement et les Matériaux (IPREM), UMR 5254, Université de Pau et des Pays de l'Adour (E2S/UPPA), Pau 64053, France*

Philippe Le Coustumer − *Bordeaux Imaging Center, UMS 3420 CNRS-INSERM, Université de Bordeaux, Bordeaux 33076, France*

Karen Gaudin − *ARNA, INSERM U1212, UMR CNRS 5320, Université de Bordeaux, Bordeaux 33076, France*

Claire Dalmay − *XLIM-UMR CNRS 7252, Université de Limoges, Limoges 87060 LIMOGES CEDEX, France*

Arnaud Pothier − *XLIM-UMR CNRS 7252, Université de Limoges, Limoges 87060 LIMOGES CEDEX, France*

Fabrice Lalloué − *EA3842-CAPTuR, GEIST, Faculté de Médecine, Université de Limoges, Limoges 87025, France*

Complete contact information is available at: https://pubs.acs.org/10.1021/acs.analchem.1c02466

Notes

The authors declare no competing financial interest.

ACKNOWLEDGMENTS

This study was supported by the European Project No. SUMCASTEC (Horizon 2020 Research and Innovation Programme under Grant Agreement No. 737164) and "Région Nouvelle Aquitaine" (2018-1R10128).

REFERENCES

(1) Cheray, M.; Begaud, G.; Deluche, E.; Nivet, A.; Battu, S.; Lalloue, F.; Verdier, M.; Bessette, B.. Cancer Stem-Like Cells in Glioblastoma. In *Glioblastoma*; De Vleeschouwer, S., Ed.; Codon Publications: Brisbane, 2017.

(2) Dawood, S.; Austin, L.; Cristofanilli, M. *Oncology* **2014**, *28*, 1101−1107.

(3) Batlle, E.; Clevers, H. *Nat. Med.* **2017**, *23*, 1124−1134.

(4) Matsui, W. H. *Medicine* **2016**, *95*, S8−S19.

(5) Chang, J. C. *Medicine* **2016**, *95*, S20−S25.

(6) Luo, M.; Li, J. F.; Yang, Q.; Zhang, K.; Wang, Z. W.; Zheng, S.; Zhou, J. J. *World J. Stem Cells* **2020**, *12*, 1307−1326.

(7) Nassar, D.; Blanpain, C. *Annu. Rev. Pathol.* **2016**, *11*, 47−76.

(8) Pan, Y.; Ma, S.; Cao, K.; Zhou, S.; Zhao, A.; Li, M.; Qian, F.; Zhu, C. *J. Cancer Res. Ther.* **2018**, *14*, 1469−1475.

(9) Singh, S. K.; Hawkins, C.; Clarke, I. D.; Squire, J. A.; Bayani, J.; Hide, T.; Henkelman, R. M.; Cusimano, M. D.; Dirks, P. B. *Nature* **2004**, *432*, 396−401.

(10) Clevers, H. *Nat. Med.* **2011**, *17*, 313−319.

(11) Kuşoğlu, A.; Biray Avcı, Ç. *Gene* **2019**, *681*, 80−85.

(12) Liou, G. Y. *Int. J. Biochem. Cell Biol.* **2019**, *106*, 1−7.

(13) Yan, Y.; Zuo, X.; Wei, D. *Stem Cells Transl. Med.* **2015**, *4*, 1033−1043.

(14) Zhu, F.; Qian, W.; Zhang, H.; Liang, Y.; Wu, M.; Zhang, Y.; Zhang, X.; Gao, Q.; Li, Y. *Stem Cell Rep.* **2017**, *9*, 429−437.

(15) Buczek, M. E.; Reeder, S. P.; Regad, T. *Methods Mol. Biol.* **2018**, *1692*, 139−148.

(16) Mohiuddin, I. S.; Wei, S. J.; Kang, M. H. *Biochim. Biophys. Acta Mol. Basis Dis.* **2020**, *1866*, 165432.
(17) Rajendran, V.; Jain, M. V. *Methods Mol. Biol.* **2018**, *1692*, 89−95.
(18) Vlashi, E.; Pajonk, F. *Semin. Cancer Biol.* **2015**, *31*, 28−35.
(19) Yakisich, J. S.; Azad, N.; Kaushik, V.; Iyer, A. K. V. *J. Cell. Physiol.* **2017**, *232*, 2280−2286.
(20) Schmohl, J.; Vallera, D. *Toxins (Basel)* **2016**, *8*, 165.
(21) Beier, C. P.; Beier, D. *Front. Biosci. (Elite Ed)* **2011**, *3*, 701−710.
(22) Mélin, C.; Perraud, A.; Akil, H.; Jauberteau, M. O.; Cardot, P.; Mathonnet, M.; Battu, S. *Anal. Chem.* **2012**, *84*, 1549−1556.
(23) Lacroix, A.; Deluche, E.; Zhang, L. Y.; Dalmay, C.; Mélin, C.; Leroy, J.; Babay, M.; Morand du Puch, C.; Giraud, S.; Bessette, B.; Bégaud, G.; Saada, S.; Lautrette, C.; Pothier, A.; Battu, S.; Lalloué, F. *Anal. Chem.* **2019**, *91*, 8948−8957.
(24) Faye, P.-A.; Vedrenne, N.; De la Cruz-Morcillo, M. A.; Barrot, C.-C.; Richard, L.; Bourthoumieu, S.; Sturtz, F.; Funalot, B.; Lia, A.-S.; Battu, S. *Anal. Chem.* **2016**, *88*, 6696−6702.
(25) Guglielmi, L.; Battu, S.; Le Bert, M.; Faucher, J. L.; Cardot, P. J. P.; Denizot, Y. *Anal. Chem.* **2004**, *76*, 1580−1585.
(26) Naves, T.; Battu, S.; Jauberteau, M.-O.; Cardot, P. J. P.; Ratinaud, M.-H.; Verdier, M. *Anal. Chem.* **2012**, *84*, 8748−8755.
(27) Mélin, C.; Lacroix, A.; Lalloué, F.; Pothier, A.; Zhang, L. Y.; Perraud, A.; Dalmay, C.; Lautrette, C.; Jauberteau, M. O.; Cardot, P.; Mathonnet, M.; Battu, S. *J. Chromatogr. A* **2013**, *1302*, 118−124.
(28) Bocca, B.; Battistini, B.; Petrucci, F. *Talanta* **2020**, *220*, No. 121404.
(29) Bousse, T.; Shore, D. A.; Goldsmith, C. S.; Hossain, M. J.; Jang, Y.; Davis, C. T.; Donis, R. O.; Stevens, J. *J. Virol. Methods* **2013**, *193*, 589−596.
(30) González-Espinosa, Y.; Sabagh, B.; Moldenhauer, E.; Clarke, P.; Goycoolea, F. M. *Int. J. Biol. Macromol.* **2019**, *136*, 911−919.
(31) Manczak, R.; Baristiran Kaynak, C.; Kaynak, M.; Palego, C.; Lalloue, F.; Pothier, A.; Saada, S.; Provent, T.; Dalmay, C.; Bessette, B.; Begaud, G.; Battu, S.; Blondy, P.; Jauberteau, M. O. *IEEE J. Electromagn. RF. Microw. Med. Biol.* **2019**, *3*, 191−198.
(32) Bégaud-Grimaud, G.; Battu, S.; Leger, D. Y.; Cardot, P. J. P.. Mammalian Cell Sorting with Sedimentation Field-Flow Fractionation. In *Field-Flow Fractionation in Biopolymer Analysis*; Williams, S. K. R.; Caldwell, K. D., Eds.; Springer-Verlag: Wien, 2012.
(33) Caldwell, K. D.; Cheng, Z. Q.; Hradecky, P.; Giddings, J. C. *Cell Biophys.* **1984**, *6*, 233−251.
(34) Stephen Williams, P.; Lee, S.; Calvin Giddings, J. *Chem. Eng. Commun.* **1994**, *130*, 143−166.
(35) Chmelík, J. *J. Chromatogr. A* **1999**, *845*, 285−291.
(36) Thankamony, A. P.; Saxena, K.; Murali, R.; Jolly, M. K.; Nair, R. *Front. Mol. Biosci.* **2020**, *7*, 79.
(37) Hussein, D.; Punjaruk, W.; Storer, L. C.; Shaw, L.; Othman, R.; Peet, A.; Miller, S.; Bandopadhyay, G.; Heath, R.; Kumari, R.; Bowman, K. J.; Braker, P.; Rahman, R.; Jones, G. D.; Watson, S.; Lowe, J.; Kerr, I. D.; Grundy, R. G.; Coyle, B. *Neuro. Oncol.* **2011**, *13*, 70−83.
(38) Pauklin, S.; Vallier, L. *Cell* **2013**, *155*, 135−147.
(39) Lathia, J. D.; Mack, S. C.; Mulkearns-Hubert, E. E.; Valentim, C. L. L.; Rich, J. N. *Genes Dev.* **2015**, *29*, 1203−1217.
(40) Borowicz, S.; Van Scoyk, M.; Avasarala, S.; Karuppusamy Rathinam, M. K.; Tauler, J.; Bikkavilli, R. K.; Winn, R. A. *J. Visualized Exp.* **2014**, *92*, No. e51998.
(41) Wang, Z.; Zhou, L.; Xiong, Y.; Yu, S.; Li, H.; Fan, J.; Li, F.; Su, Z.; Song, J.; Sun, Q.; Liu, S. S.; Xia, Y.; Zhao, L.; Li, S.; Guo, F.; Huang, P.; Carson, D. A.; Lu, D. *Br. J. Pharmacol.* **2019**, *176*, 3390−3406.

https://doi.org/10.1021/acs.analchem.1c02466
Anal. Chem. 2021, 93, 12664−12671